www.gondwanags.org.in

Research Article

ISSN : 2455-1953

JGSR
Journal of Geosciences Research
Vol. 11, No.2, July, 2026, pp. 134-144

Probability Mapping of Geochemical Dispersions: A Simpler Geostatistical Approach for Processing and Interpretations of Large Data Sets of Stream Sediments

Amrit Chandan Patra[1], Annie Daliya N.[2] and Bibhas Sen[3]

[1]*Geological Survey of India, Southern Region, Hyderabad-500068, Telangana, India*
[2]*Geological Survey of India, Training Institute, Hyderabad-500068, Telangana, India*
[3]*Geological Survey of India, State Unit: Maharashtra, Pune-411006, Maharashtra, India*
*(*Corresponding Author, E-mail: bibhas.sen@gsi.gov.in)*

Abstract

The present study provides an effective geostatistical methodology for extracting high-confidence information from geochemical stream sediment data collected on a grid-based sampling pattern over large areas. Unlike traditional deterministic interpolation methods, our approach employs exploratory data analysis of metal oxides to determine critical thresholds by examining the variability and anisotropy factors through variogram analysis of spatial data. To minimize the '*nugget effect*,' which often causes predicted values to fall below critical thresholds, kriging with probability output surfaces was applied to generate geochemical probability maps indicating the likelihood of each oxide exceeding its statistically derived threshold. The methodology was tested using stream-sediment geochemical dispersion data from the Sittampundi Layered Anorthosite Complex (SAC) and the Ramagiri–Penakacherla Schist Belt (RPS). In the SAC, probable zones exceeding critical thresholds were delineated for Fe_2O_3, CaO, MgO, Ni, Co, and Cr based on 200 samples. Similarly, in the RPS, the method effectively identified such zones for Fe_2O_3, TiO_2, CaO, MgO, and MnO using 770 samples. These case studies demonstrate the utility of geostatistically derived probability maps in delineating geochemical dispersion patterns from systematically collected stream-sediment data over extensive areas.

Keywords: Geostatistics, Kriging, Probability Mapping, Geochemical Dispersion

Introduction

Geochemical surveys and mapping are widely utilized methodologies in mineral exploration at various stages due to their cost-effectiveness and applicability across multiple mapping scales (Tolosana-Delgado and Boogaart, 2014). In mineral and mining exploration, geochemical studies are generally divided into two distinct stages. The first involves the collection and examination of various geological materials, including rocks, soils, and stream sediments. The second stage entails plotting geochemical values on maps, analyzing the numerical data, and interpreting the results (Paz-Ferreiro *et al.,* 2010). Proper analysis of the acquired geochemical data enables the extraction of information about the underlying geology, alteration zones, weathering patterns, and other geological processes, thereby supporting the preparation of regional geological maps (Selia *et al.,* 2019). Historically, such techniques have been among the most productive tools in mineral prospecting, particularly through the application of stream-sediment geochemical surveys (McClenaghan *et al.,* 2011). In this context, stream-sediment analysis serves as a valuable method for identifying potential areas for future exploration.

To delineate prospective zones for mineral exploration, the Geological Survey of India (GSI) has accumulated an extensive geochemical database over the past two decades (2001 onwards) For each composite sample, chemical analyses were done in the NABL-accredited laboratories of GSI. Details of analytical procedures and standards used for NGCM samples are provided in Table 1. With the accumulation of such large-scale geochemical datasets, it becomes essential to employ robust statistical methods for effective visualization and identification of significant spatial patterns and continuities.

In general, statistical analysis of geochemical data requires an understanding of both the geological setting and principles of Statistics. Typically, exploratory data analysis is employed to determine the critical threshold of elements from stream-sediment data (Reimanna *et al.,* 2005). The final step in data processing involves creating an interpolated surface from the sampled data and mapping regions where element concentrations exceed the

(Received : 26 October 2025 ; Revised Form Accepted : 12 April 2026)
https://doi.org/10.56153/g19088-025-0290-110

Table 1: The analytical procedures and standards used for NGCM samples

Analytical Method	Description
ICP-MS Fusion Method: Geochemical Analysis of Geological Samples	0.10 g of accurately weighed geological sample mixed with 0.15g Lithium Tetraborate and 0.15 g anhydrous Lithium Metaborate into platinum crucibles. Then mix the sample thoroughly without any spillage. The platinum crucible is placed in Muffle furnace and heated up to 1050°C for one hour. The fused material is dissolved by adding 25 ml of 8% HNO3 (AR) and using a magnetic stirrer. Transferred the solubilized contents into 250 ml of volumetric flask and added Indium as an internal standard solution (5 ml of 500 ppb) and then added 100 ml of 8% HNO3 (AR). Finally, the solution is made up to 250 ml with ultrapure water. The sample is analyzed for REE and Trace elements using Agilant make ICP-MS (7700 Series) using calibration standards and blank solutions. Calibration standards and blank solutions are also prepared using the same method as described above for samples. The calibration standards used for calibration are GSD-3a, GSD-9, and GSD-11 and the check standard used is GSD-6.
ICP-MS Acid Digestion Method: Geochemical Analysis of Geological Samples	Take 0.25 g. sample in teflon beaker add 10 ml of aqua-regia slowly and is mixed thoroughly and add 5 ml Hydrofluoric Acid (48% Merk (GR)) and mix slowly (by rotation) and leave the contents aside overnight with the covered lid on hot plate. Next day add 5 ml of Perchloric acid and evaporate the contents to the syrupy stage. Dissolve the syrupy paste in 5 ml aqua-regia by heating for about 30 min in closed lid then cool the solution. This solution is made up to 25 ml in a graduated test tube with MQ water and mix thoroughly. This is stock solution. From this stock was taken 2 ml and made up to 20 ml with 2% HNO3 by the addition of Rhodium as internal standard at 10 ppb in the final solution. The diluted solution is measured for Mo, In, Cs, W, Tl, Bi, Sb, Te, Li by ICP-MS with standard GSD-6 and GSD-12 used for calibration and the check standard used was GSD-5a.
XRF pressed pellets method: Geochemical Analysis of Geological samples	Additive Binder Powder Pack Technique: (-200) Mesh sample is taken for preparation of Pressed pellets. Pellets of each sample are prepared by mixing 4.5g sample with 0.3g wax powder (Starch, wax, cellulose, etc.) It is thoroughly mixed and put into aluminum disc and pressed in the mechanical pressed pellet machine at pressure 20 pound. These pellets are numbered and used for analysis. Different International calibration standards like GSD-2, GSD-3, GSD-4, GSD-5, GSD-7, GSD-8, GSD-10, GSD-11, GSS-1, GSS-3, GSS-4, GSS-6, GSS-10, and GSS-11 are used for calibration of instrument. Wavelength dispersive X-Ray Fluorescence Spectrometer- WDXRF (Make: PANalytical, Model: AXIOS MAX), used for the non-destructive analysis of major oxides, minor and trace elements in geological samples.
AAS-GTA (Agilent-200 series) method: Geochemical Analysis of Geological samples	Estimation of Ag and Cd: Take 0.5 g sample in 50 ml glass beaker. Add 6-7 ml (1:1) HNO_3 into the beaker. Digest on hot plate (slow-medium) for 2 hours covered with watch glass. Now evaporate to syrupy mass by removing the watch glass. Make up to 20ml with 5% nitric acid, keep it overnight. Estimate Ag & Cd. Prepare standards of 2, 4, 6 ppb of silver and cadmium using 10ppb stock solution using auto command of the instrument for calibration of instrument. Prepare Processed Blank and SRM's in the similar manner. Graphite tube atomizer- Atomic Absorption Spectrophotometer – GTA-AAS (Make: Agilent, Model: 200 series AA), used for the analysis of Silver and Cadmium in geological samples. Estimation of Gold: Take 20 g sample in 50 ml porcelain dish. Roast at 650^0C. Roasted sample is transferred in 250 ml glass beaker. Add 20 ml aqua-regia, keep it overnight. Heat up to syrupy mass on the hot plate. Make up to 100 ml with 20% HCl and kept for settling. Transfer5 0ml of the aliquot in 125 ml separating funnel and add 10 ml MIBK, shake, discard the aqueous layer. Wash the organic layer twice with 5% HCl, collect the MIBK layer in 25ml glass-stopper test tube. Shake & keep it for the estimation of Au by GTA-AAS. Standards 10, 20, 30 ppb are used for Calibration of Instrument which is made by using bulk solution of 50 ppb automatically.

determined critical thresholds. This facilitates geological interpretation relevant to the study area and supports delineation of zones for subsequent stages of mineral exploration.

As a geostatistical tool for analyzing spatially distributed geological and geochemical data, ordinary kriging generates an exact prediction surface at sampled locations with minimal deviation (Cressie, 1988; Wackernagel, 1998; Paz-Ferreiro *et al.,* 2010). However, due to the nugget effect, the predicted surface may exhibit reduced range values and increased error variance (Kresic and Mikszewski, 2013). This limitation complicates the demarcation of spatial distributions exceeding critical thresholds, which is a key objective of stream-sediment–based geochemical prospecting aimed at identifying potential mineralization zones. While recognizing the potential of simulation-based methods for complex geological environments, this study focuses on a simpler, probability-based kriging approach.

Against this backdrop, the present study employs geostatistical kriging as a tool for probability-based mapping to: (a) define critical threshold values of selected elements from stream-sediment geochemical data in relation to the geological setting, and (b) generate geochemical probability prediction maps showing areas where elemental concentrations exceed the statistically determined thresholds.

Methodology

The methodology was tested in two distinct geological settings, the Sittampundi Layered Igneous Complex, Tamil Nadu, and the Ramagiri-Penakacherla Schist Belt, Andhra Pradesh. The geostatistical approach proved effective in classifying these study areas into zones exceeding critical thresholds, thereby providing indirect indications of elemental enrichment or depletion related to mineralization.

The geochemical dataset of major oxides and trace elements was obtained from the National Geoscience Data Repository (NGDR) portal, a freely accessible database maintained by the (Geological Survey of India, 2023; https://geodataindia.gov.in). The study area corresponds to a topographic sheet the covers a rectangular area of approximately 720 km² in Peninsular India (Ramagiri, Sitampundi, *etc.),* comprising 196 composite stream-sediment analyses, each representing an area of 4 km².

After organizing the dataset for the area of interest in a spreadsheet (*e.g.,* Microsoft Excel), the following steps of preliminary statistical and geostatistical analysis were undertaken.

Step- 1

The statistical evaluation based on concepts of the frequency distribution of elemental concentrations (reflecting the relative occurrence and range of values) and spatial distribution of individual elements treated as variables. Basic univariate and bivariate analyses of the major oxides and trace elements were followed by statistical examination of multi-element correlations, pattern recognition, and subsequent modeling and interpretation (Grünfeld, 2005).

To evaluate the significance of correlations among variables, the critical value of the Student's t statistic was calculated (Davis, 2002).

$$t_c = (r/\sqrt{1-r}) \times \sqrt{n-2}$$

In geoscientific applications, for n > 30 and a probability level of 0.05 (95% confidence), correlations are considered significant when $t_c > 3$ (Davis, 2002).

A crucial aspect of traditional statistical approaches is the determination of critical thresholds. The conventional calculation of thresholds as the mean ± 2 standard deviations (mean ± 2σ) assumes normally distributed, independent samples (Carranza, 2009). Therefore, before estimating critical thresholds, it is essential to visually examine the data distribution using exploratory data analysis (EDA).

In this study, we employed a robust and non-parametric approach Median ± 2MAD (Median plus or minus twice the Median Absolute Deviation) to determine the critical threshold (Reimanna *et al.,* 2005). This method is less sensitive to outliers and typically yields lower threshold values, thereby identifying a greater number of anomalous samples.

Step-2

The geostatistical analysis was conducted to generate a continuous interpolated surfaces from the spatially distributed sample points, incorporating spatial autocorrelation at defined intervals within the study area. The Geostatistical Analyst extension of ArcMap was employed for this purpose. In addition to various interpolation techniques, this extension provides several diagnostic tools for evaluating and interpreting data, thereby facilitating the generation of optimal prediction surfaces based on available data.

The selected dataset was processed to compute an experimental semivariogram, followed by variogram model fitting, neighborhood search, cross-validation, and surface prediction using kriging interpolation techniques. Fitting of the variogram model was based on directional variograms, which have a significant influence on spatial prediction. Global trends (Fig. 1) and Anisotropy (Fig. 2) representing directional influences in the semivariogram, greatly affect the output surface (Johnston *et al.*, 2001). Initially, ordinary kriging with prediction surfaces was used to generate continuous interpolated maps and contour lines. To account for global trends, detrending procedures were applied to extract all relevant spatial information and maximize the capabilities of the Geostatistical Analyst extension (Kresic and Mikszewski, 2013). The zones exceeding the critical threshold (Median ± 2MAD) were demarcated by classifying the contour lines derived from the interpolated surface.

However, due to the nugget effect, ordinary kriging acts as an inexact interpolator, resulting in a reduction of the range and accumulation of error variance (Kresic and Mikszewski, 2013). Consequently, the predicted surface showed reduced maximum values sometimes below the estimated critical threshold thereby limiting the ability to delineate areas exceeding that threshold.

To address this issue, ordinary kriging with probability output surfaces was performed to produce geochemical probability maps of oxides exceeding their respective critical thresholds. Probability kriging, a binary-variable approach, utilizes indicator kriging, where measured values are first converted into binary form (indicating whether they are above or below a threshold). These binary values are then interpolated to generate a surface representing the probability of exceeding the threshold (Kresic and Mikszewski, 2013). While indicator kriging estimates the probability of exceedance directly, probability kriging combines indicator and cokriging approaches to improve prediction accuracy and better represent the spatial distribution of zones exceeding critical thresholds (Johnston *et al.,* 2001).

Results

The geostatistical approach detailed in the Methodology section was applied to two distinct geological provinces *i.e.* Case

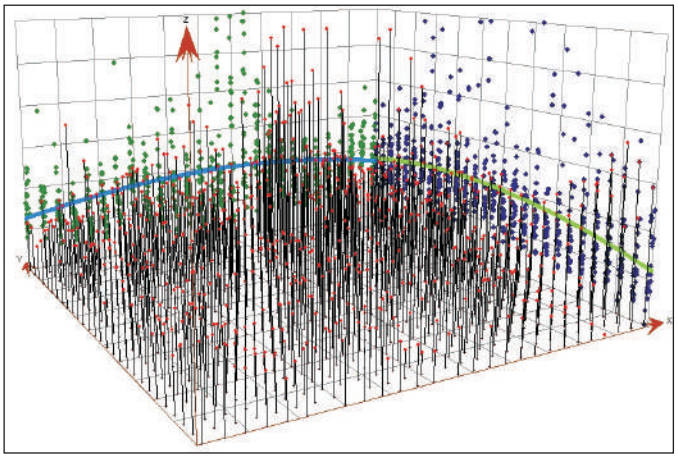

Fig. 1. Directional variogram of Fe_2O_3 with Global trend phenomena (RPS study area)

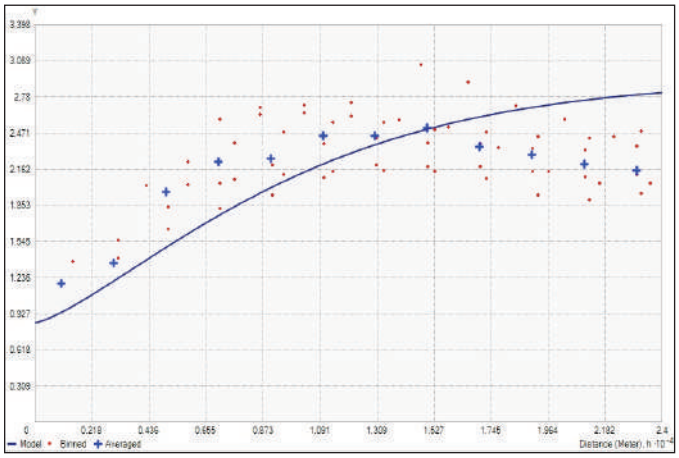

Fig. 2. Directional variogram of Fe_2O_3 showing Anisotropy (RPS study area)

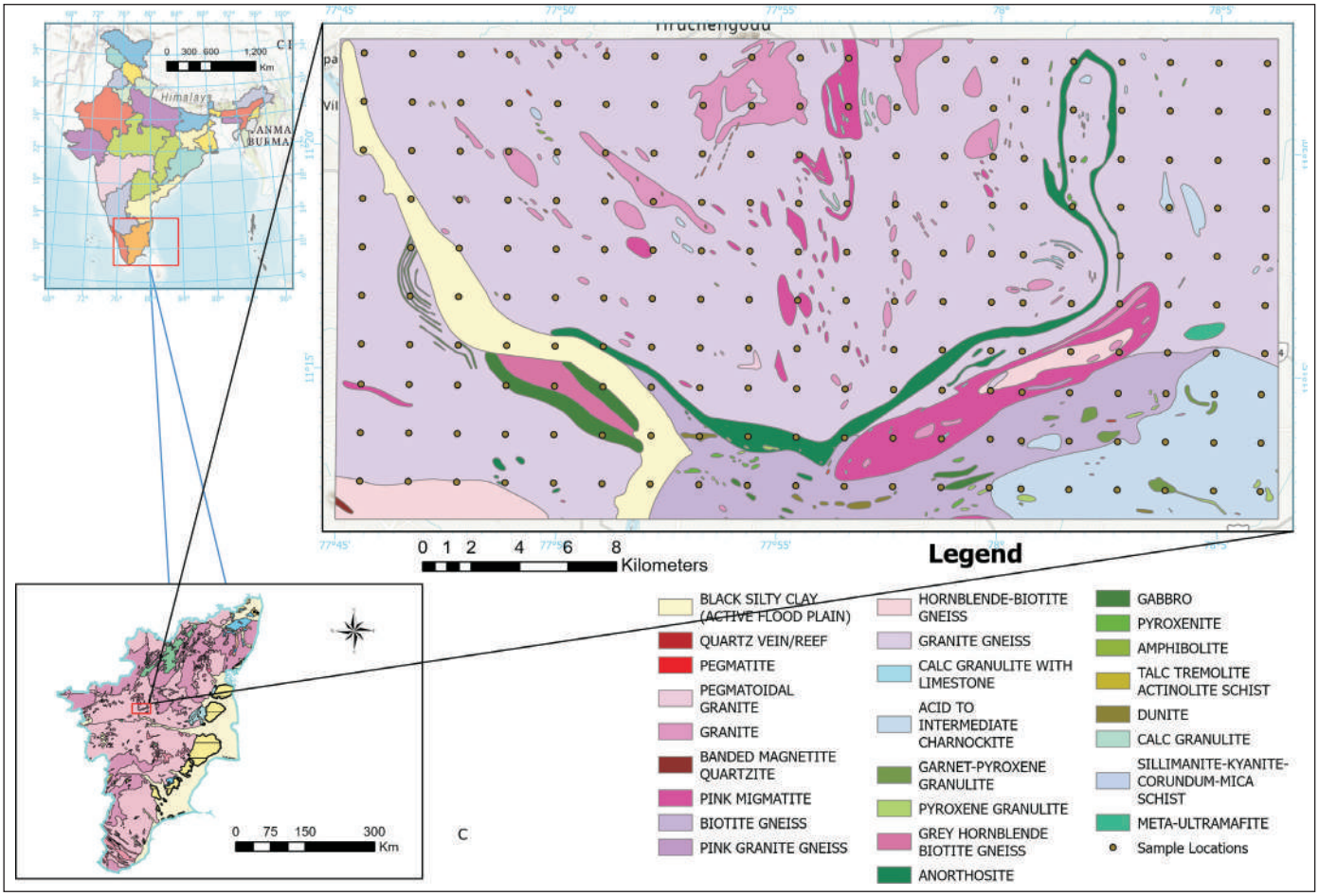

Fig. 3. Location map of Sittampundi Layered Anorthosite Complex, Tamil Nadu (Source: Geological Survey of India, 2024, Compiled 1: 50000)

Study 1: The Sittampundi Layered Anorthosite Complex (SAC) in the Southern Granulite Terrain, Tamil Nadu, and Case Study 2**:** The Ramagiri–Penakacherla Schist Belt (RPS) in the Eastern Dharwar Craton, Andhra Pradesh.

The locations of the stream-sediment samples used in this study are shown in SAC (Fig. 3) and RPS (Fig. 4).

Sittampundi Layered Anorthosite Complex

Geological Setting

The Archaean Sittampundi Layered Anorthosite Complex (SAC) of Tamil Nadu comprises anorthosite interlayered with bands and lenses of chromitite, chrome–spinel-bearing pyroxenite, garnet–pyroxene granulite, and amphibolite (Fig.3). The complex has undergone high-grade metamorphism, ranging from upper amphibolite to granulite facies, and is exposed as tectonic lenses within the Cauvery Shear Zone (Sesha Sai *et al.,* 2009). The lithological assemblages of SAC occur along an arcuate belt hosted within a granodiorite–tonalite gneiss complex. Older metamorphic inclusions such as garnet–kyanite–biotite gneiss, banded magnetite quartzite, and metapyroxenite are also associated with this gneissic suite (Nathan and Balukkarasu, 2009).

The complex forms a broad arcuate belt, varying in width from ~125 to 990 m and extending for about 17 km along strike (Dhanendran *et al.,* 2014). It comprises meta-gabbro to meta-pyroxenite and hornblende–meta-anorthosite layers intercalated with chromitite and meta-anorthosite. These lithological variations correspond with systematic changes in major and trace element geochemistry (Bhaskar Rao *et al.,* 1996; Janardhan and Leake, 1975).

Structurally, SAC represents a tectonically reworked remnant of a layered igneous intrusion that has been extensively recrystallized and deformed. It is preserved within ductile quartzofeldspathic gneisses that have undergone considerable finite strain. The complex has been folded into an isoclinal antiform, producing stratigraphic duplication across both limbs, locally separated by gneissic rocks. Later open folding modified this structure, resulting in the present interference pattern geometry (Ramadurai *et al.,* 1975).

Geochemical Database-A

The SAC geochemical database comprises major and minor oxides (in wt%) and trace elements (in ppm), covering an area of approximately 800 km².

Descriptive/Preliminary statistical analysis

Univariate and bivariate statistical analyses of the major oxides and trace elements (Fe_2O_3, CaO, MgO, Ni, Co, and Cr) were performed using Microsoft Excel. The statistical summaries for Case Study 1 are presented in Table 2 and Table 3, while corresponding data for Case Study 2 are provided in Table 4 - 5.

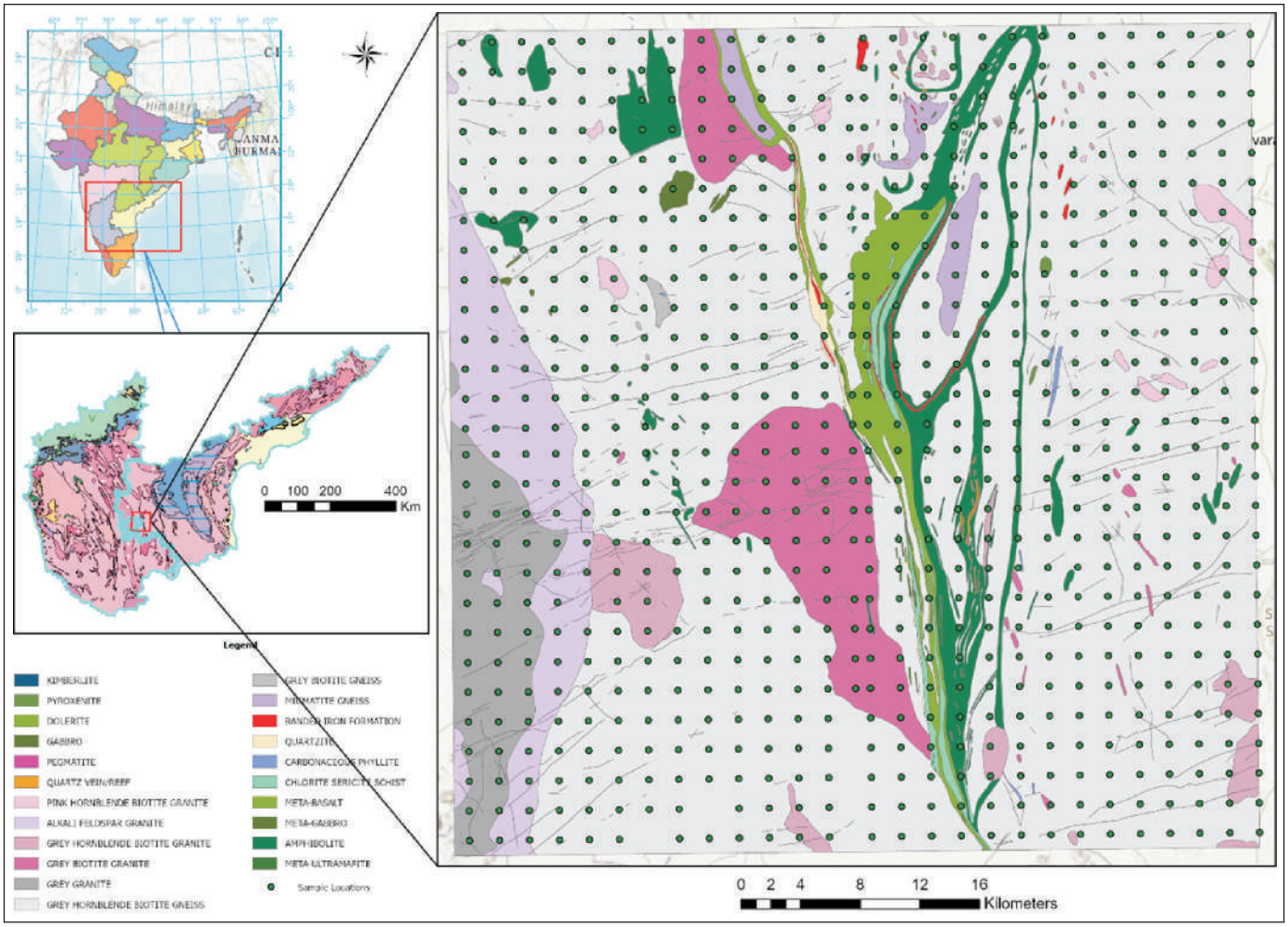

Fig. 4. Location map of the Ramagiri Schist Belt, Andhra Pradesh (area) (Source: Geological Survey of India, 2024; Compiled 1: 50000)

The significant correlation between the major oxides and some trace elements is shown in 3 for the SAC area.

Based on significant correlations among the major oxides and their geological relevance, three major oxides (Fe_2O_3, CaO, MgO) and three trace elements (Ni, Co, and Cr) were selected for further geostatistical analysis. Threshold values for these elements, computed using the Median ± 2MAD method (Reimanna *et al.*, 2005) are summarized in Table 5.

Geostatistical Analysis

As outlined in the Methodology, geostatistical analysis was

Table 2: Summary Statistics of Major Oxides (SAC)

	SiO_2	Fe_2O_3	TiO_2	CaO	MgO	MnO	Na_2O
Mean	55.99	7.37	0.69	4.88	3.96	0.61	1.96
Median	56.16	7.13	0.74	4.52	3.40	0.09	2.14
Standard Deviation	3.38	1.50	0.37	1.64	1.77	1.05	0.63
Variance	11.45	2.26	0.14	2.70	3.13	1.10	0.39
Kurtosis	0.43	-0.08	-0.08	0.50	3.57	1.10	-0.14
Skewness	-0.38	0.54	-0.07	0.74	1.81	1.65	-0.89
Minimum	44.78	4.15	0.06	1.45	1.80	0.05	0.51
Maximum	65.03	11.87	1.74	10.99	11.91	3.97	3.10
Count	200	200	200	200	200	200	200

Table 3: Correlation coefficient of Major Oxides (After Pearson's) (SAC)

Pearson's r	Fe_2O_3	CaO	MgO	Ba	Ni	Co	Cr
Fe_2O_3	-	0.343	0.473	-0.725	0.633	0.616	0.627
CaO	0.343	-	0.026	-0.298	0.303	0.106	0.183
MgO	0.473	0.026	-	-0.560	0.404	0.618	0.479
Ba	-0.725	-0.298	-0.560	-	-0.617	-0.563	-0.662
Ni	0.633	0.303	0.404	-0.617	-	0.647	0.897
Co	0.616	0.106	0.618	-0.563	0.647	-	0.524
Cr	0.627	0.183	0.479	-0.662	0.897	0.524	-

Table 4: Significant correlation of major oxides (Case study 1)

T test	Fe_2O_3	CaO	MgO	Ba	Ni	Co	Cr
Fe_2O_3	NA						
CaO	5.14	NA					
MgO	7.56	0.37	NA				
Ba	-14.79	-4.39	-9.51	NA			
Ni	11.51	4.47	6.21	-11.03	NA		
Co	11.00	1.50	11.06	-9.58	11.93	NA	
Cr	11.33	2.62	7.68	-12.43	28.62	8.67	NA

Table 5: Threshold values of selected oxides and trace elements of SAC area

Elements	Fe_2O_3	MgO	Ni	Co	Cr	CaO
Median	7.125	3.395	55.9	19.7	125.1	4.52
MAD	0.98	0.71	13.5	4	34.3	2.195
Threshold	9.085	4.815	82.9	27.7	193.7	8.91

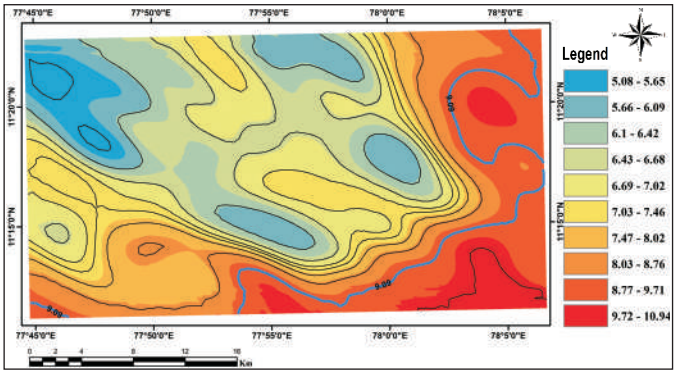

Fig. 5. Interpolation of Fe_2O_3 with prediction Kriging (SAC study area)

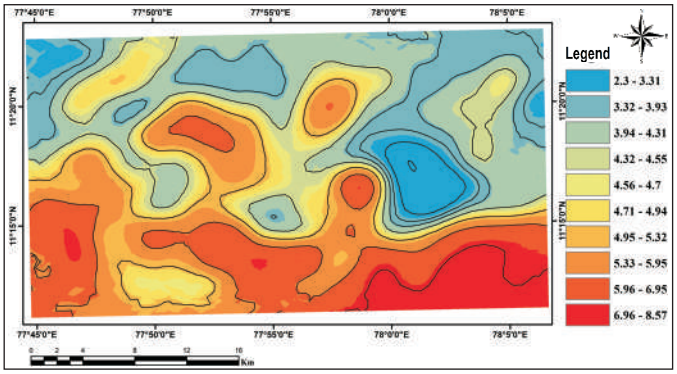

Fig. 7. Interpolation of CaO with prediction Kriging (SAC study area)

performed using the Geostatistical Analyst tool in ArcMap© to generate interpolated prediction surfaces. For Fe_2O_3, the calculated threshold was 9.09%, and the prediction range contracted from 4.15–11.87% to 5.08–10.94%. Similarly, the range for MgO was 1.95–9.16%, Ni ranged between 20.55–28.8 ppm, Co between 6.43–9.09 ppm, and Cr between 85.41–413.74ppm. The zones exceeding the critical thresholds were delineated as blue contours (Fig. 5).

In contrast, the range of predicted CaO values shrank from 1.45–10.99% to 2.30–8.57%, with a threshold value of 8.91%, preventing the delineation of zones above the critical threshold using ordinary kriging alone.

Salient Understanding from Geostatistical Data Processing in Case Study -1

Mapping geochemical data above critical thresholds is a primary objective of any geochemical study. For SAC, this was achieved using ordinary kriging prediction surfaces for all variables except CaO.

For Fe_2O_3, the calculated threshold (9.09%) was below the maximum predicted value (10.94%), allowing delineation of areas exceeding the threshold (Fig. 5). However, where prediction ranges contracted below the threshold, such as for CaO, this approach failed, as the predictive model yielded a narrow concentration range that remained entirely below the threshold value, resulting in no spatially distinguishable anomalous zones.

To address this, ordinary kriging with probability output surfaces was employed. For example, using Fe_2O_3 as a reference, a probability surface was generated for the threshold value of 9.09%, and the red zones (Fig. 6) corresponded closely with the ordinary kriging contours (blue zones in figure 5). Similar consistency was observed across other variables (Fig. 13a-h). For CaO, probability kriging successfully delineated threshold-exceeding zones (Fig. 8).

The prediction and probability surfaces recovered valuable information regarding the underlying geology, alteration, and weathering patterns. The Fe_2O_3 and MgO distributions correspond well with the ferro-magnesian lithounits, whereas CaO mirrors the distribution of calc-granulite rocks. These spatial correspondences assist in narrowing target zones for mineral exploration.

Ramagiri-Penakacherla Schist Belt

Geological Setting

The second case study encompasses parts of the Ramagiri–Penakacherla Schist Belt (RPS) in the Anantapur District of Andhra Pradesh. The RPS, part of the Eastern Dharwar Craton (EDC), is a late Archaean, volcanics-dominated greenstone belt well known for its gold mineralization (Zachariah *et al.,* 1996). The belt trends NNW–SSE, extending for about 120 km, with a variable width of 0.25–2.7 km.

The belt comprises volcaniclastic metasedimentary rocks such as amphibolite–chlorite–sericite schists, metagreywackes, argillites, phyllites, siliceous shales, and auriferous quartz veins. Minor gabbroic intrusions and banded ferruginous quartzites (BFQ)

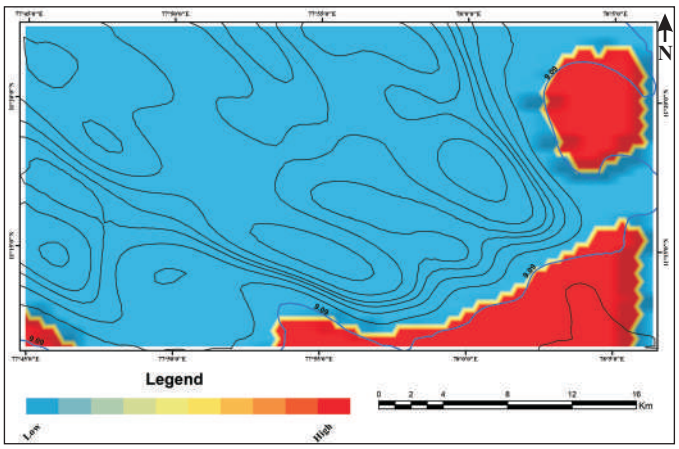

Fig. 6. Interpolation of Fe_2O_3 with probability Kriging (SAC study area)

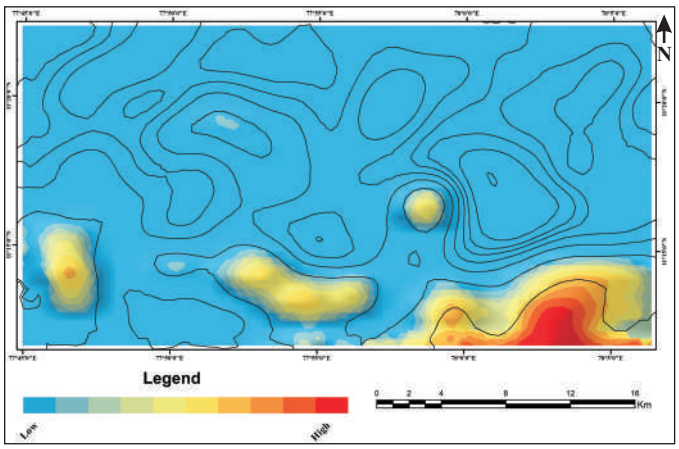

Fig. 8. Interpolation of CaO with probability Kriging (SAC study area)

also occur (Yellappa and Chetty, 2008; Zachariah *et al.,* 1997). These lithological units display intense folding and moderate metamorphism typical of the Dharwarian sequence (Ghose *et al.,* 1970).

Structurally, the belt exhibits a Y-shaped outcrop pattern dominated by mafic volcanic rocks enveloped by Peninsular Gneiss (Deb and Konka, 2005). Gold–quartz vein mineralization occurs primarily within sheared, chlorite–carbonate–rich phyllitic zones, bounded by strongly deformed and mylonitized granitic gneisses that form high-strain shear zones exceeding 100 km in length, marking a transition from brittle to ductile deformation.

Geochemical Database-B

The RPS geochemical database comprises major oxides (wt%) and trace elements (ppm), covering an area of approximately 3,000 km².

Descriptive/Preliminary Statistical Analysis

Univariate and bivariate analyses of major oxides were carried out using Microsoft Excel, and results are summarized in Table 6-8. Threshold values, computed using the Median ± 2MAD method (Reimann *et al.,* 2005), are listed in Table 9.

The bivariate analysis of major oxides for case study 2 are shown in Table 7.

The significant correlation of the major oxides is shown in for Case study 2.

Based on significant correlations among the major oxides and geological context, four major oxides (Fe_2O_3, TiO_2, CaO, and MgO) were selected for detailed analysis. MnO was also included to demonstrate the effectiveness of probability kriging in delineating zones exceeding critical thresholds.

Geostatistical Analysis

The results for RPS mirrored those of the SAC. For Fe_2O_3, the critical threshold was 5.88%, with a prediction range contracting from 1.30–12.38% to 2.12–10.29%. For TiO_2, CaO, and MgO, the prediction ranges were 0.03–0.17%, 0.18–5.72%, and 1.16–8.38%, respectively.

The range shrinkage was attributed to the nugget effect, as discussed previously.

The delineated zones above the critical thresholds are shown

Table 6: Summary Statistics of Major Oxides (RPS Belt)

	SiO_2	Al_2O_3	Fe_2O_3	TiO_2	CaO	MgO	MnO	Na_2O	K_2O	P_2O_5
Mean	63.42	15.22	4.58	0.06	1.47	2.96	2.25	2.69	0.68	0.12
Median	63.64	15.30	4.26	0.06	1.35	2.74	2.26	2.66	0.64	0.10
Standard Deviation	4.47	1.23	1.64	0.03	0.65	1.19	0.49	0.81	0.29	0.07
Variance	20.01	1.52	2.68	0.00	0.42	1.42	0.24	0.66	0.09	0.01
Kurtosis	1.45	1.67	4.41	10.44	5.49	2.11	4.28	0.45	61.30	31.11
Skewness	-0.44	-0.64	1.72	2.74	1.73	1.30	0.37	0.21	5.65	4.58
Minimum	44.10	9.80	1.30	0.02	0.18	1.16	0.59	0.38	0.18	0.03
Maximum	78.53	20.27	12.38	0.23	5.72	8.38	5.97	5.04	4.72	0.88
Count	770	770	770	770	770	770	770	770	770	770

Table 7: Correlation coefficient of Major Oxides (*after* Pearson's) (RPS Belt)

Pearson's r	SiO_2	Al_2O_3	Fe_2O_3	TiO_2	CaO	MgO	MnO	Na_2O	K_2O	P_2O5
SiO_2	-	-0.046	-0.594	-0.494	-0.532	-0.511	0.363	0.401	-0.318	-0.256
Al_2O_3	-0.046	-	0.320	0.145	0.083	0.052	0.243	0.224	0.085	0.154
Fe_2O_3	-0.594	0.320	-	0.892	0.763	0.640	-0.415	-0.514	0.669	0.283
TiO_2	-0.494	0.145	0.892	-	0.763	0.589	-0.449	-0.567	0.630	0.095
CaO	-0.532	0.083	0.763	0.763	-	0.741	-0.369	-0.594	0.416	0.210
MgO	-0.511	0.052	0.640	0.589	0.741	-	-0.219	-0.567	0.389	0.308
MnO	0.363	0.243	-0.415	-0.449	-0.369	-0.219	-	0.399	-0.260	0.027
Na_2O	0.401	0.224	-0.514	-0.567	-0.594	-0.567	0.399	-	-0.287	0.097
K_2O	-0.318	0.085	0.669	0.630	0.416	0.389	-0.260	-0.287	-	0.331
P_2O_5	-0.256	0.154	0.283	0.095	0.210	0.308	0.027	0.097	0.331	-

Table 8: Significant correlation of major oxides (Case study 2)

T test	SiO_2	Al_2O_3	Fe_2O_3	TiO_2	CaO	MgO	MnO	Na_2O	K_2O	P_2O_5
SiO_2	NA									
Al_2O_3	-1.24	NA								
Fe_2O_3	-19.82	9.06	NA							
TiO_2	-15.26	3.95	52.90	NA						
CaO	-16.84	2.23	31.70	31.70	NA					
MgO	-15.96	1.38	22.34	19.56	29.60	NA				
MnO	10.44	6.73	-12.26	-13.50	-10.64	-6.04	NA			
Na_2O	11.76	6.17	-16.06	-18.47	-19.80	-18.47	11.67	NA		
K_2O	-9.00	2.29	24.17	21.74	12.26	11.31	-7.24	-8.03	NA	
P_2O_5	-7.11	4.18	7.92	2.56	5.75	8.68	0.73	2.62	9.40	NA

Table 9 : Threshold values of selected oxides (case study 2)

Oxide	Fe_2O_3	TiO_2	CaO	MgO	MnO
Median	4.26	0.06	1.35	2.735	2.26
MAD	0.81	0.01	0.36	0.685	0.57
Threshold	5.88	0.08	2.07	4.11	3.40

as blue contours in Figures 21–23. However, in cases such as MnO, where the prediction range (1.32–3.40%) contracted below the calculated threshold (3.40%), the objective of identifying threshold-exceeding zones could not be achieved using ordinary kriging alone.

To overcome this limitation, ordinary kriging with probability output surfaces was applied to generate geochemical probability maps of oxides and trace elements.

Salient Understanding from Geostatistical Data Processing in Case Study -2

As observed in Case Study 1, both prediction and probability kriging surfaces were generated to delineate zones above critical thresholds. For Fe_2O_3, with a threshold of 5.88% and a maximum predicted value of 10.29%, the exceedance areas were marked by blue contours (Fig. 9). However, for MnO (threshold 3.40%; maximum predicted 3.49%), threshold delineation was not feasible using prediction surfaces alone (Fig. 11). The application of probability kriging successfully delineated these zones as red probability contours (Fig. 12).

The probability surfaces revealed spatial patterns that closely mimic the underlying geological framework. Fe_2O_3 (Fig. 10) corresponds with the distribution of banded iron formations (BIF), while TiO_2 (Fig. 14 a-f) strongly correlated with Fe_2O_3 exhibits a similar spatial trend. These geostatistical outputs enhance the interpretation of the region's lithological and alteration patterns and provide valuable guidance for delineating target zones for mineral exploration.

Discussion

Geochemical mapping provides essential insights into underlying geological processes and remains one of the most effective tools in mineral exploration. However, deterministic interpolation approaches often fail to capture the true geological controls on elemental distribution, as directional influences cannot be effectively incorporated during interpolation. This limitation can be mitigated through geostatistical techniques, particularly kriging, which explicitly account for spatial correlation structures in the interpolation process.

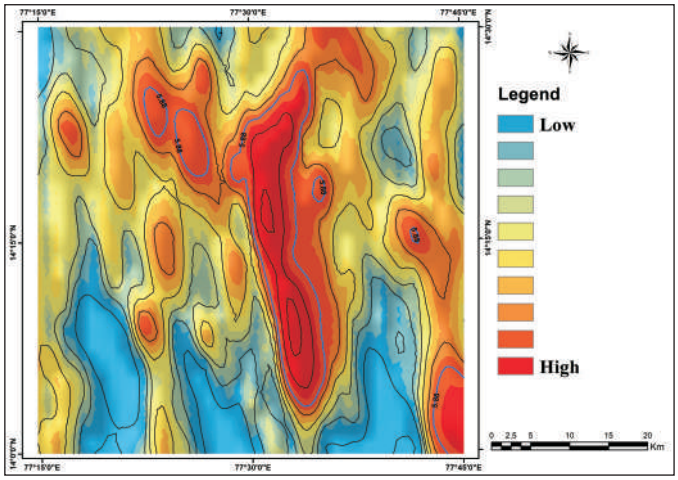

Fig. 9. Interpolation of Fe_2O_3 with prediction Kriging (RPS study area)

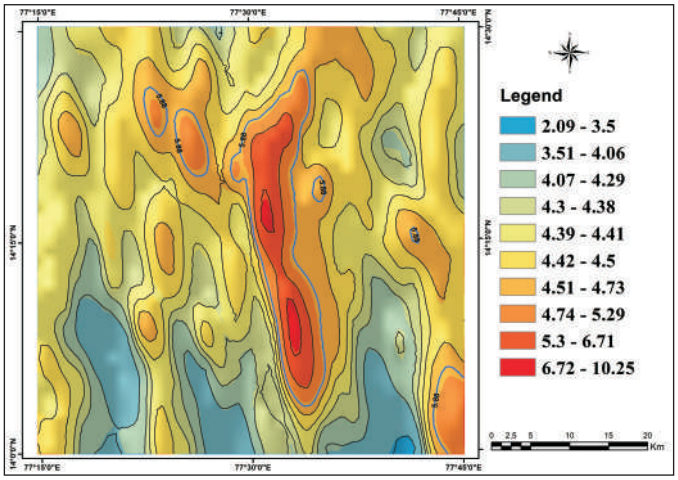

Fig. 10. Interpolation of Fe_2O_3 with prediction Kriging (RPS study area)

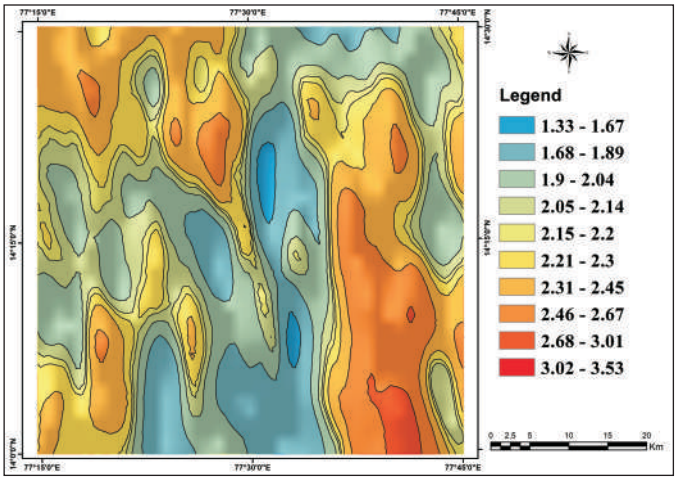

Fig. 11. Interpolation of MnO with prediction Kriging (RPS study area)

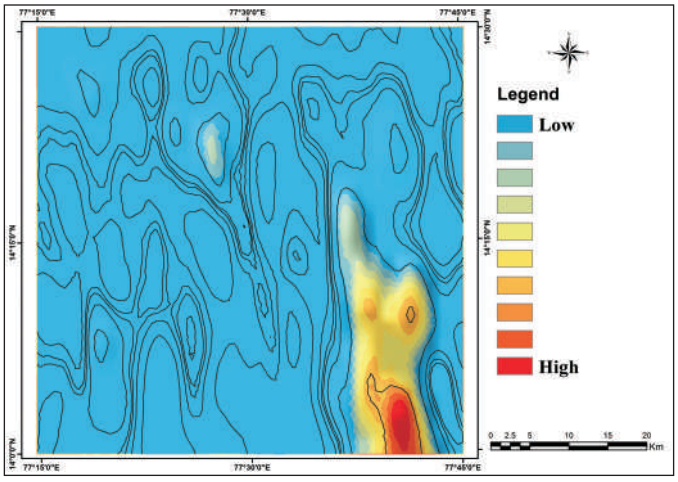

Fig. 12. Interpolation of MnO with probability Kriging (RPS study area)

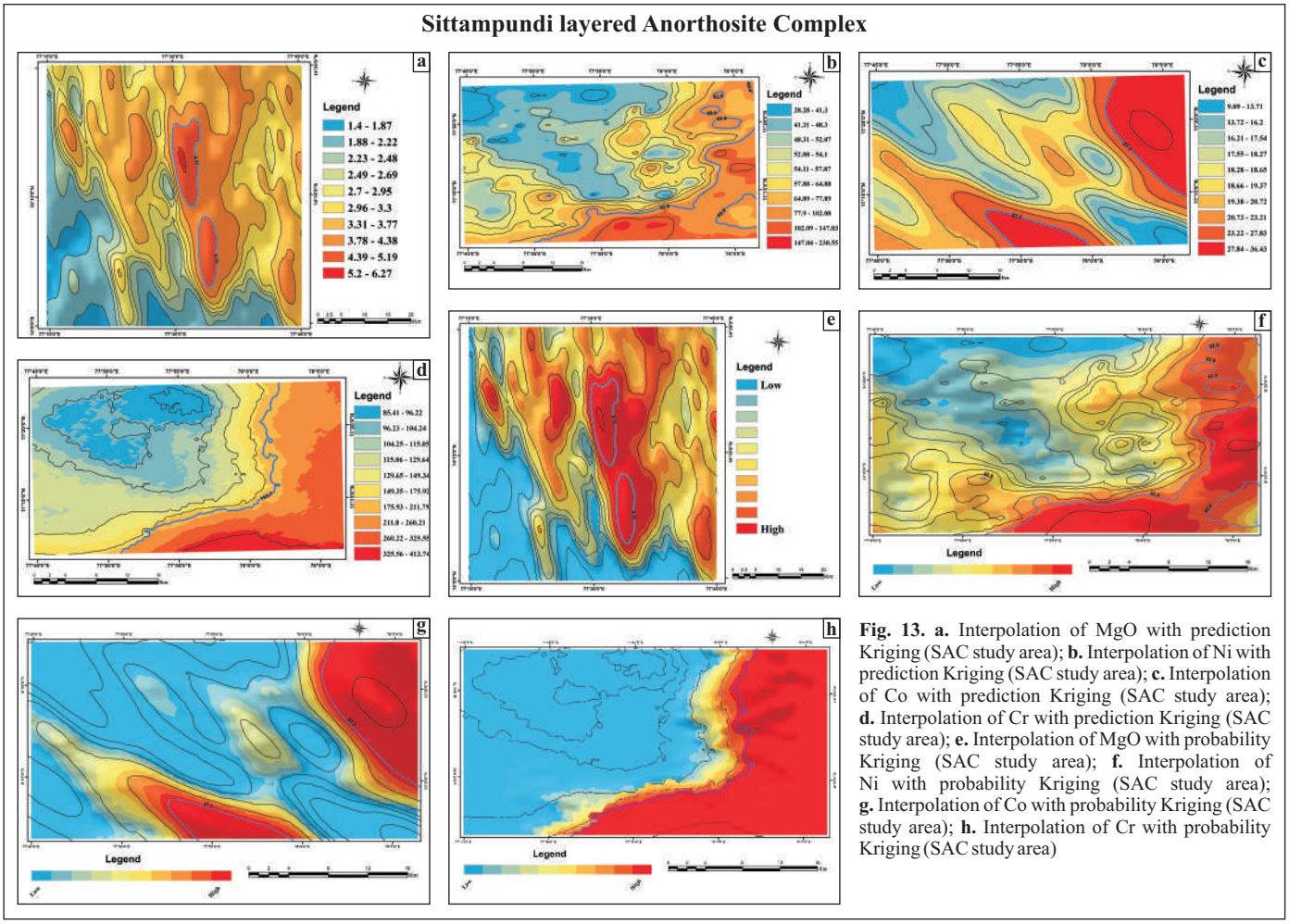

Fig. 13. a. Interpolation of MgO with prediction Kriging (SAC study area); **b.** Interpolation of Ni with prediction Kriging (SAC study area); **c.** Interpolation of Co with prediction Kriging (SAC study area); **d.** Interpolation of Cr with prediction Kriging (SAC study area); **e.** Interpolation of MgO with probability Kriging (SAC study area); **f.** Interpolation of Ni with probability Kriging (SAC study area); **g.** Interpolation of Co with probability Kriging (SAC study area); **h.** Interpolation of Cr with probability Kriging (SAC study area)

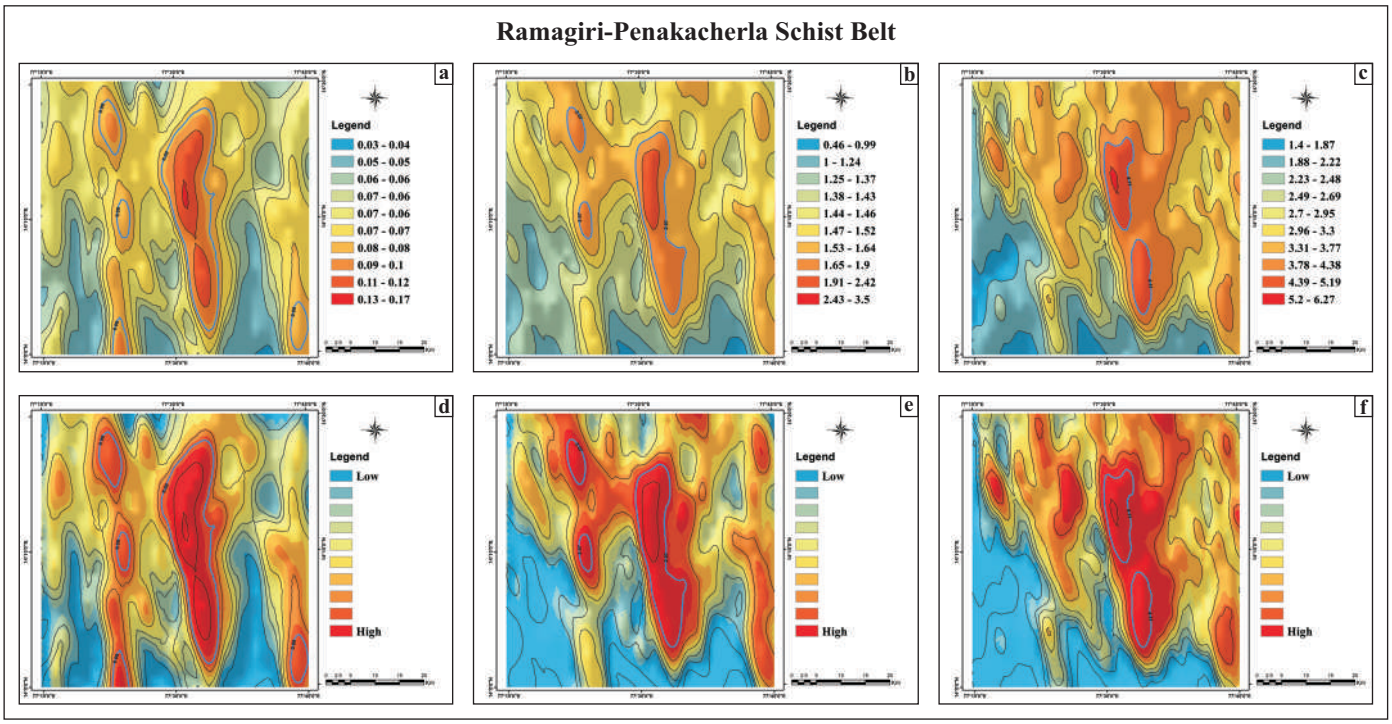

Fig. 14. a. Interpolation of TiO_2 with prediction Kriging (RPS study area); **b.** Interpolation of CaO with prediction Kriging (RPS study area); **c.** Interpolation of MgO with prediction Kriging (RPS study area); **d.** Interpolation of TiO_2 with probability Kriging (RPS study area); **e.** Interpolation of CaO with probability Kriging (RPS study area); **f.** Interpolation of MgO with probability Kriging (RPS study area)

In this study, ordinary kriging with prediction surfaces was applied to generate elemental distribution maps for both study areas the Sittampundi Layered Anorthosite Complex and the Ramagiri–Penakacherla Schist Belt. Zones exceeding the calculated critical thresholds were delineated as prospective areas, providing valuable guidance for further exploration. Probability kriging maps additionally revealed potential environmental and geological controls influencing spatial distributions. For instance, Fe_2O_3, MgO, Ni, Co, Cr, and CaO exhibited systematic spatial patterns in the Sittampundi Anorthosite Complex, whereas Fe_2O_3, TiO_2, CaO, MgO, and MnO showed similar trends in the Ramagiri–Penakacherla Schist Belt. Anomalous zones for Ni and Cr corresponded closely with the known disposition of the anorthosite bands, while Fe_2O_3 and TiO_2 anomalies aligned with the distribution of banded ferruginous quartzites. These correlations demonstrate the capability of probability kriging to effectively delineate geochemical anomalies consistent with known lithological and mineralization patterns.

The study underscores that geostatistical methods are particularly effective for classifying exploration areas into zones exceeding critical thresholds and for distinguishing similarities and contrasts in mineralization processes. However, the reliability of such analyses depends heavily on accurate threshold estimation and the careful construction of directional variograms, including the assessment of trends and anisotropy, followed by rigorous cross-validation of variogram models. These procedures are essential to ensure precision and to minimize uncertainty in the delineation of anomalous zones.

Beyond the present case studies, the broader significance of geochemical data processing lies in its contribution to understanding geological processes and their geochemical manifestations. The methodology demonstrated here provides a robust and reproducible framework that, when integrated with geological insight and statistical rigor, facilitates reliable anomaly identification and enhances mineral prospectivity assessments.

It is pertinent to note that recent research by Li *et al.* (2021) highlighted inherent limitations of interpolation-based approaches such as kriging, particularly their tendency to smooth spatial variability and obscure localized geochemical anomalies. They proposed an integrated framework combining multiple-point geostatistical simulation (MPS) with local singularity analysis (LSA), enabling multiple realizations to capture spatial uncertainty and, through singularity–quantile analysis, to produce anomaly probability maps that better represent geological controls.

Nevertheless, the present study demonstrates that geostatistical kriging, particularly when combined with probability mapping, remains a practical and efficient approach for processing stream-sediment geochemical data to infer the controls of underlying lithological units. The methodology outlined herein enables readers and practitioners to interpret geological phenomena effectively, while remaining cognizant of its inherent limitations. Integrating this approach with regional or local geological knowledge allows for the judicious selection of variables and enhances the interpretive value of subsequent statistical and spatial analyses.

Conclusions

This study highlights the efficacy of geostatistical probability mapping as a practical and reliable tool for processing and interpreting large stream-sediment geochemical datasets. Using ordinary kriging, spatial prediction surfaces were generated for selected major and trace elements from two contrasting geological settings—the Sittampundi Layered Anorthosite Complex and the Ramagiri–Penakacherla Schist Belt. Zones exceeding statistically defined critical thresholds were identified, providing insights into areas of potential mineralization and their relationship with underlying lithological units. The spatial distributions of elements such as Fe_2O_3, MgO, Ni, Co, Cr, and CaO in the Sittampundi Complex, and Fe_2O_3, TiO_2, CaO, MgO, and MnO in the Ramagiri–Penakacherla Belt, showed close correspondence with known geological features. These results demonstrate the capability of probability kriging to delineate geochemical anomalies consistent with established lithological and mineralization patterns. The study emphasizes that reliable results of a geostatistical analyses depend on accurate threshold estimation, robust variogram modelling, and appropriate consideration of anisotropy. Despite its inherent smoothing effect, kriging remains computationally efficient and effective for regional geochemical assessments. While newer approaches such as multiple-point simulation and singularity analysis can better capture spatial uncertainty, ordinary kriging integrated with probability mapping offered a balanced framework combining simplicity, reproducibility, and interpretive power. As exemplified here by, this methodology provides a sound basis for translating geochemical data into meaningful geological interpretations and for guiding future mineral exploration.

Authors' Contributions

ACP: Conceptualization, Designing the Methodology, Formal Analysis and Writing. **ADN**: Data Collection and Processing, Software, Validation and Visualization. **BS**: Supervision, Writing, Revision and Editing.

Conflict of Interests

All the authors declare that they have no conflicts of interest in the subject matter or materials discussed in this manuscript.

Acknowledgments

The authors express their sincere gratitude to the Deputy Director General, Training Institute, Geological Survey of India, Hyderabad, for facilitating this work during the period when all three authors served as faculty members at the Centre for Geoinformatics Management and Training. The authors also acknowledge the Director, Chemical Division, Geological Survey of India, Southern Region, Hyderabad, for providing information on the analytical procedures and standards employed for NGCM samples.

References

Bhaskar Rao, Y.J., T.R.K. Chetty and A.S. Janardhan (1996). Sm-Nd and Rb-Sr ages and P-T history of the Archean Sittampundi and Bhavani layered meta-anorthosite complexes in Cauvery shear zone, South India: evidence for Neoproterozoic reworking of Archean crust. Contrib. Mineral. Petrol., v.125, pp. 237–250.

Carranza, Emmanuel and John, M. (2009). Geochemical Anomaly and Mineral Prospectivity Mapping in GIS. Amsterdam, The Netherlands: Elsevier 368p.

Cressie, Noel (1988). Spatial prediction and ordinary kriging. Mathemat. Geol., v. 20, pp. 405-421.

Davis, John C. (2002). Statistics and Data Analysis in Geology. 3rd Edition. New York: John Wiley & Sons, 656p.

Deb, Mihir and Konka, B. (2005). Stable isotope geochemistry of the gold-sulfide mineralized zone of the Kottapalle block of the Ramagiri greenstone belt, Dharwar Craton, South India. Mineral Deposit Research: Meeting the Global Challenge. Beijing: Springer, pp. 743-746.

Dhanendran, S., Nathan, N.P., Vijay Kumar, R., Pillai, L.M.P. and Balukkarasu, A. (2014). Chromite and Sulphide Hosted PGE Mineralisation in Sittampundi Layered Anorthosite Complex, Tamil Nadu. Jour. Geol. Soc. India, v.2, pp. 1-8.

Geological Survey of India (2023.). GSI OCBIS Portal. Government of India, Kolkata. 6 August. https://geodataindia.gov.in.

Geological Survey of India (2024). Geological Map, GSI Bhukosh. Compiled 1: 50000, 16 July. https://bhukosh.gsi.gov.in/Bhukosh.

Ghose, D.B., Sastry, B.B.K., Rao, A.J. and Rahim, A.A. (1970). Ore Environmenta nd Ore Genesisin RamagiriG old Field, Andhra Pradesh, India. Econom. Geol., pp. 801-814.

Grünfeld, Katrin (2005). Visualization, integration and analysis of multi-element geochemical data. Stockholm: TRITA-LWR PhD Thesis 54p.

Janardhan, A.S., and Leake, B.E. (1975). The origin of the meta-anorthositic gabbros and garnetiferous granulites of the Sittampundi complex, Madras, India. Jour. Geol. Soc. India, v.16(4), pp. 391-408.

Johnston, Kevin, Krivoruchki, K., Ver Hoef, J.M. and Lucas, N. (2001). Using ArcGIS Geostatistical Analyst. New York Street, Redlands: ESRI, 306p.

Kresic, N. and Mikszewski, A. (2013). Hydrogeological conceptual site models: data analysis and visualization. Boca Raton: CRC Press, 585p.

Li, Cheng, Bingli Liu, Ke Guo, Li Binbin and Yunhui Kong (2021). "Regional Geochemical Anomaly Identification Based on Multiple-Point Geostatistical Simulation and Local Singularity Analysis—A Case Study in Mila Mountain Region, Southern Tibet." Minerals 11: 1037 pp. 1-14.

McClenaghan, M.B., Grunsky, E.C. and Chork, C.Y. (2011). Regional stream sediment geochemistry in mineral exploration. Geochem.: Explor., Environ. Anal., v.11, pp.99–121.

Nathan, N.P. and Balukkarasu, A. (2009). Survey for Platinum Group of Elements in Sittampundi layered Mafic-Ultramafic Complex. Rec. Geol. Surv. India, v.141(5).

Paz-Ferreiro, Jorge, Eva Vidal Vázquez and Sidney Rosa Vieira (2010). Geostatistical Analysis of a Geochemical dataset. Bragant. Campin., pp. 121-129.

Ramadurai, S., Sankaran, M., Selvan, T.A. and Windley, B.F. (1975). The Stratigraphy and Structure of the Sittampundi Complex, Tamil Nadu, India. Jour. Geol. Soc. India, v.16(4), pp. 409–414.

Reimanna, Clemens, Peter Filzmoserb and Robert G. Garrettc (2005). Background and threshold: critical comparison of methods of determination. Sci. Tot. Environ., v.346, pp.1-16.

Selia, Sangga Rima Roman, Raimon Tolosana-Delgado, Purnama Sendjaja, K. Gerald van den Boogaart and Helmut Schaeben (2019). Geostatistical Compositional Analysis of Regional Geochemical Stream Sediments of West Java, Indonesia. Joint Convention Yogyakarta. Yogyakarta pp. 1-6.

Sesha Sai, V.V., N.P. Nathan, R.V. Vijay Kumar and Balukkarasu, A. (2009). Occurrence of PGE minerals in Archaean Sittampundi layered Anorthosite Complex, Tamil Nadu, South India. Indian Jour. Geosci., v.63(2), pp. 305-310.

Tolosana-Delgado, Raimon and Gerald van den Boogaart, K. (2014). Towards compositional geochemical potential mapping. Jour. Geochem. Explor., pp. 42-51.

Wackernagel, Hans (1998). Multivariate Geostatistics: An Introduction with Applications. France: Springer, 235p.

Yellappa, T. and Chetty, T.R.K. (2008). Mafic Dykes Around Ramagiri Schist Belt, East Dharwar Craton, South India: Possible Palaeo Stress Regimes. INDIAN DYKES: Geochem., Geophys. Geochronol., pp.1-19.

Zachariah, J.K., Mohanta, M.K. and Rajamani, V. (1996). Accretionary Evolution of the Ramagiri Schist Belt, Eastern Dharwar Craton. Jour. Geol. Soc. India, v.47, pp. 279–291.

Zachariah, John K., Rajamani, V. and Gilbert N. Hanson (1997). Petrogenesis and source characteristics of metatholeiites from the Archean Ramagiri schist belt, eastern part of Dharwar Craton, India. Contrib. Mineral. Petrol., pp. 87-104.